Atomic-scale design of radiation-tolerant nanocomposites

M.J. Demkowicz, P. Bellon, and B.D. Wirth

Recent work indicates that materials with nanoscale architectures, such as nanolayered Cu-Nb composites and nanoscale oxide dispersion-strengthened steels, are both thermally stable and offer improved performance under irradiation. Current understanding of the atomic-level response of such materials to radiation yields insights into how controlling composition, morphology, and interface-defect interactions may further enable atomic-scale design of radiation-tolerant nanostructured composite materials. With greater understanding of irradiation-assisted degradation mechanisms, this bottom-up design approach may pave the way for creating the extreme environment–tolerant structural materials needed to meet the world's clean energy demand by expanding use of advanced fission and future fusion power.

Introduction

Structural materials used in nuclear reactors must withstand some of the harshest conditions met in existing technology. All of the factors limiting their lifetime and performance at high temperatures and in corrosive media, such as creep and stress corrosion cracking, are exacerbated by irradiation.[1,2] These materials are also subject to degradation by mechanisms distinctive to radiation environments, such as volumetric swelling and anisotropic growth.[3,4]

Decades of traditional alloy development have yielded incremental enhancements in materials performance under irradiation.[5] Advanced fission and future fusion reactor designs, however, call for far more dramatic progress, such as materials able to sustain radiation doses up to 10 times higher than in current reactors while withstanding liquid metal corrosion[6] or being implanted with up to several atomic percent of helium.[7]

The last several decades have also witnessed major advances in our understanding of the atomic-scale origins of material behavior under irradiation[8,9] thanks to improvements in experimental techniques such as high-resolution transmission electron microscopy and atom probe tomography (APT), as well as computer modeling techniques such as classical potential molecular dynamics (MD) and density functional theory. This knowledge provides a foundation for the emergence of first-principles, atomic-scale design of materials for radiation resistance.

In contrast to purely hit-and-miss materials development, atomic-scale design aims to achieve superior radiation response by purposefully manipulating composition and microstructure to control the behavior of radiation-induced defects. It relies on modeling to determine the impact of these modifications on engineering-level material behavior. Atomic-scale design is being used today to accelerate the improvement of existing materials. In the longer term, however, it seeks to realize unconventional materials that could not have arisen through a series of gradual modifications.

Although only a fledgling in the area of structural materials, atomic-scale design has already shown success in other energy-related fields, such as the search for novel battery electrode materials.[10] (See the article by Gerbrand Ceder in the September 2010 issue of the *MRS Bulletin*.) This article illustrates how atomic-scale design for radiation resistance is being pursued in the tailoring of radiation-resistant interfaces, design of stable microstructures, and development of nanostructured ferritic alloys (NFAs). Challenges facing this approach to materials engineering are also discussed.

Atomic-level origin of radiation damage

The topic of radiation effects in structural materials encompasses a vast literature dating from 1942[11] and cannot be fully reviewed in this article. It is well understood, however, that the root causes of radiation damage are individual and clustered

M.J. Demkowicz, Massachusetts Institute of Technology, Cambridge, MA 02139, USA; demkowicz@mit.edu
P. Bellon, University of Illinois at Urbana-Champaign, Urbana, IL 61801, USA; bellon@illinois.edu
B.D. Wirth, University of Tennessee, Knoxville, TN 37996, USA; bdwirth@utk.edu

vacancies and self-interstitials produced during collisions between energetic particles and target atoms.[12] The subsequent diffusion and clustering of these defects, along with the associated transport of impurities, lead to accelerated creep,[1] volumetric swelling,[3] segregation of alloying elements,[13] and embrittlement.[14] Furthermore, the forced atomic mixing taking place in the displacement cascades themselves can lead to disordering of chemically ordered phases and to dissolution of precipitates.[15] These processes can severely limit material and component lifetimes in radiation environments.

In addition to clustering and diffusing, radiation-induced vacancies and interstitials also may recombine if they come close enough to each other. Since both defects are annihilated in the process, recombination may be thought of as a "self-healing" mechanism. Thus, enhancing vacancy-interstitial recombination is one of the strategies for improving the radiation resistance of crystalline materials discussed in the examples that follow.

Tailored interfaces

Interfaces are efficient sinks and recombination sites for radiation-induced point defects,[16] so it may be possible to improve the radiation resistance of many materials by increasing their interface area per unit volume, for instance, by refining their grain size using severe plastic deformation. (See the Zhu et al. and Raabe et al. articles in this issue.) Interfaces with differing atomic structures, however, may exhibit disparate sink strengths,[17,18] diffusivities,[19] mechanical properties,[20] and susceptibilities to embrittlement.[21] Moreover, interfaces also increase the free energy of a material and, in some cases, may be its weakest microstructural link, limiting its overall lifetime.[22] For enhanced performance under irradiation, it is therefore not sufficient for a material to contain a large number of interfaces; they must also be of the right kind.

Interface structure and properties are functions of crystallographic misorientation, habit-plane direction, properties of the adjacent materials such as crystal structure, cohesive energy, elastic constants, and many other factors. Atomic-scale design of interfaces is the judicious selection of these parameters to obtain interfaces with desired properties. Since the design space afforded by these parameters is infinite, a hit-and-miss approach can never exhaust it. Design of interfaces for radiation resistance therefore requires an understanding of the connection between their structure and the mechanisms of their interaction with point defects. Recent work on fcc-bcc heterophase interfaces in Cu-Nb multilayer composites affords an example of how modeling and experiments can describe this connection and how it may be applied for atomic-scale design.

Cu-Nb multilayer composites can be synthesized as thin films by magnetron sputtering with individual layer thicknesses from hundreds of nanometers to as thin as 1 nm. Thanks, in part, to the limited solubility of Cu and Nb (see following section), these composites are thermally stable up to 800°C.[23] Their response to radiation has been studied between room temperature and 1200°C using He-ion bombardment at energies between 33 keV and 150 keV and fluences up to 1.5×10^{17} ions/cm^2.[24] Some of these experiments were produced in excess of 10 displacements per atom (dpa). (At 1 dpa, every atom in the material has been displaced once, on average, by a collision with a high-energy particle.[25])

The Cu-Nb multilayers remain morphologically stable under these conditions, with no mixing or amorphization detected.[26,27] Their radiation-induced defect concentrations are far below those of pure fcc Cu and bcc Nb subjected to similar dpa levels, as shown in **Figure 1**, and decrease with decreasing thickness of the individual layers, with increasing interface area per unit volume. Thus, radiation resistance of these materials can be unambiguously attributed to interfaces. Thanks to the distinctive microstructure of magnetron-sputtered Cu-Nb multilayers, all the heterophase interfaces found in them are nearly identical,[28] a fact that makes them an ideal model system for investigating interface–point defect interactions. An atomic model of a Cu-Nb bilayer containing one interface constructed according to the experimentally observed crystallography is shown in **Figure 2a**.

MD modeling using a specially constructed Cu-Nb-embedded-atom–method potential has shown that the number of point defects created in collision cascades near Cu-Nb interfaces is about 50–70% smaller than in pure Cu or Nb,[29] confirming that these interfaces are excellent point-defect sinks. The remaining defects may subsequently diffuse to interfaces and become trapped as well. Under steady-state irradiation in the absence of other defect sinks, equal numbers of vacancies and interstitials arrive at the interfaces and undergo accelerated recombination, effectively healing radiation damage.

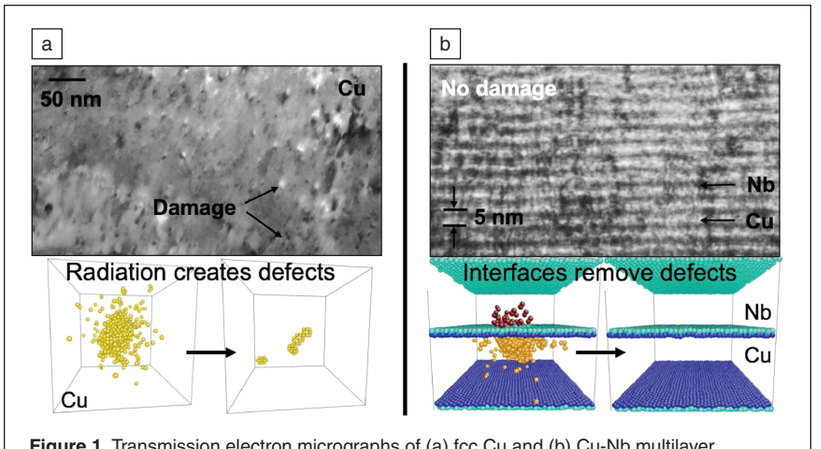

Figure 1. Transmission electron micrographs of (a) fcc Cu and (b) Cu-Nb multilayer composites implanted with 150 keV He to a dose of 10^{17} ion/cm^2. Radiation-induced defects created in collision cascades accumulate in pure Cu but are trapped and recombined at Cu-Nb interfaces, as illustrated in the lower panels.[26,27,29]

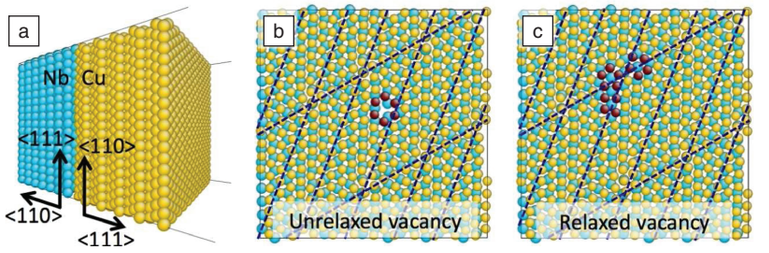

Figure 2. (a) Simulated Cu-Nb bilayer with the same crystallography as observed experimentally in multilayer composites.[28] (b) An unrelaxed vacancy (red atoms) in the Cu interface plane (c) migrates to the nearest intersection between misfit dislocations (dashed lines) and causes a local interface reconstruction (red atoms).[30,31]

Investigation of the atomic structure of Cu-Nb interfaces reveals the reason for their high efficiency in trapping point defects. Figure 2b shows a plane view of the interfacial Cu and Nb. While this interface has no strict periodicity, it nevertheless contains a quasi-periodic pattern of low coordination sites where a Cu atom and a Nb atom are situated nearly one on top of the other. This quasi-periodicity arises from the presence of two sets of parallel interface misfit dislocations.[30,31] The low coordination sites occur at the intersections between misfit dislocations.

Figure 2b shows a vacancy created in the interfacial Cu plane by removing an atom. Before relaxation, this defect is compact, like conventional vacancies found in perfect crystals. Annealing for 10 ps at 300 K, followed by conjugate gradient energy minimization, however, leads to the interface reconstruction shown in Figure 2c. In it, the vacancy migrates to the nearest misfit dislocation intersection and delocalizes over an area of about 2 nm^2. Its formation energy drops by about 1.6 eV in the process. Introduction of interstitials into a Cu-Nb interface leads to the same kind of interface reconstruction.[30,31] If both a vacancy and an interstitial are formed in the vicinity of the same misfit dislocation intersection, they undergo spontaneous recombination as they relax.

Misfit-dislocation intersections are therefore both trapping sites and recombination centers for radiation-induced defects absorbed at Cu-Nb interfaces. This insight suggests that interfaces could be tailored for radiation resistance, for example by maximizing the number of misfit-dislocation intersections in them. The areal density of these intersections can be obtained through analytical investigation of the Frank-Bilby equation[31,32]

$$\bar{\mathbf{b}} = (\mathbf{I} - \mathbf{F}^{-1})\,\hat{\mathbf{p}}, \qquad (1)$$

which specifies the average Burgers vector content per unit length $\bar{\mathbf{b}}$ along a unit vector $\hat{\mathbf{p}}$ in the plane of an interface. Here, $\mathbf{F}$ is the deformation gradient that characterizes the misorientation and misfit between the two crystals that meet at the interface, and $\mathbf{I}$ is the identity tensor. The number of trapping sites in an interface is therefore primarily a function of interface crystallography, which may be controlled by appropriate synthesis techniques.

Considerations besides interface geometry, such as misfit dislocation core width or the elastic properties of the materials that meet at the interface, are likely to enter into this atomic-scale design strategy as studies on more interfaces are conducted. Under some conditions, for example, overlap between dislocation cores may render the misfit-dislocation model inapplicable. This design approach also may be extended to tailoring interface properties other than point defect sink strength, such as diffusivity, cohesive strength, or embrittlement resistance.

Stable microstructures

Nanostructured materials may coarsen, either during thermal annealing or when subjected to external forcing such as irradiation or severe plastic deformation. Coarsening during thermal annealing is not surprising since these materials may contain a significant amount of excess free energy, owing to the large volume fraction of interfaces. In the presence of irradiation or other external forcing, however, the microstructural evolution is no longer driven solely by the reduction of excess free energy, and coarsening may be enhanced or suppressed. Under appropriate irradiation conditions, nanostructured states, in fact, can become stable steady states, thus providing for intrinsic resistance against coarsening.

Several strategies can be envisioned to suppress coarsening of nanostructures under thermal annealing by lowering the coarsening driving force and the relevant mobility. The driving force is directly controlled by the interfacial free energy, while the coarsening kinetics is largely controlled either by the mobility of the interfaces or by the long-range transport of alloying elements. A first approach is therefore to use alloying elements that segregate at interface boundaries so as to reduce the interfacial energy. For instance, in the case of nanograined materials, this can be achieved by adding Fe to Y (References 33 and 34), P to Ni (Reference 33), or W to Ni (Reference 34). The resulting nanograined materials are thermodynamically metastable. Recently, the possibility of obtaining thermodynamically stable systems with vanishing grain boundary energy also has been discussed.[33,35,37]

Secondly, for two-phase materials, metastable nanostructures can be obtained by restricting interfaces to be planar, with zero average curvature. Such planar interfaces can, for instance, be synthesized by physical vapor deposition, as discussed previously for Cu-Nb nanolayers, or by accumulative roll bonding. Unlike some naturally occurring layered microconstituents such as pearlite, these structures are free from necks connecting chemically identical layers, thus improving their resistance to coarsening.

Thirdly, dispersion of long-lived nanoscale precipitates can be achieved, as in the case of nanostructured ferritic steels

discussed in the following section. The very low solubility of the precipitating elements (e.g., Y, Ti, and O) combined with their low diffusivity in the Fe matrix lead to nanostructures that, even though not thermodynamically stable or metastable, are apparently remarkably long-lived even at high temperatures.

Under irradiation, the resistance to coarsening of the previously mentioned nanostructures may be reduced, owing to point defect supersaturation, sustained point defect and chemical fluxes to interfaces, and to the forced mixing produced by energetic displacement cascades. An alternative route to the synthesis of radiation-resistant nanostructures takes advantage of irradiation-induced self-organization reactions at the nanoscale. Examples of these self-organization reactions triggered by irradiation are (1) the stabilization of ordered gamma prime precipitates a few nanometers in diameter in a gamma matrix in Ni-Al alloys;[35] (2) the formation of void and bubble lattices in many metals and alloys (see Reference 36 for a review); and (3) the patterning of nanoscale phases in immiscible alloy systems,[37–41] for instance in Cu-Ag, Cu-Fe, Cu-Co, Cu-Nb, Cu-Mo, and Cu-W.

Self-organization reactions are of particular interest, as they result in a high density of semi-coherent or incoherent interfaces, which may serve as point defect sinks, as discussed in the previous section. In the case of moderately immiscible elements such as Cu-Ag, Cu-Co, and Cu-Fe, the self-organization is rationalized by a dynamic competition between medium-scale chemical mixing forced by displacement cascades and coarsening driven by thermally activated transport.[37] Accordingly, the temperature range over which nanoscale patterning takes place can be shifted to a higher temperatures by using slow diffusers. This has been confirmed experimentally in Cu-based binary alloys, see **Figure 3**. The maximum temperature for patterning, however, remains limited for these alloy systems.

Much higher patterning temperatures are experimentally obtained by using highly immiscible alloy systems, such as Cu-Nb, Cu-Mo, and Cu-W, see **Figure 4**. Precipitate sizes around 3 to 6 nm and Cu grain sizes around 20 to 30 nm are measured during irradiations up to 75 dpa at temperatures up to 600°C for Cu-Nb and 800°C for Cu-W (i.e., 85% of the melting temperature of the Cu matrix). A different rationalization needs to be invoked in these systems, because recoil mixing is highly reduced or negligible since little or no mixing takes place during thermal spikes, owing to the immiscibility of these elements in the liquid state.[42] Vo et al.[40] have recently proposed that the observed nanostructuring results from the coagulation of small solute clusters during thermal spikes. At intermediate temperatures, thermal coarsening is suppressed due to the low solubility and low diffusivity of the Nb, Mo, and W solute atoms in Cu. As a result, the maximum precipitate size should be dictated by the cascade size, a prediction that is in good agreement with MD simulation results. Work is in progress to assess the resistance of these nanostructures to creep under irradiation and to swelling in the presence of He atoms.

The identification of the control parameters responsible for spontaneous nanoscale patterning of precipitates under irradiation makes it possible to guide the design of radiation-resistant

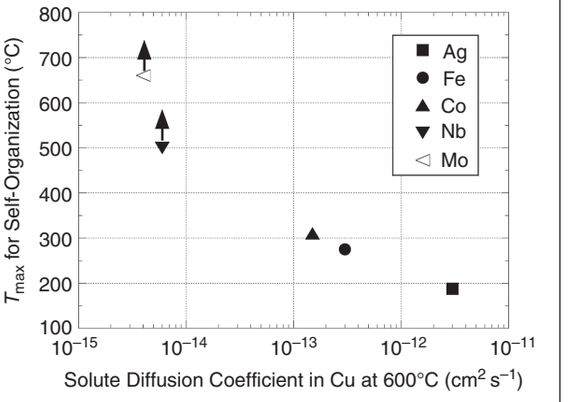

Figure 3. A comparison of the maximum temperature for self-organization during irradiation with 1.8 MeV Kr with the solute diffusion coefficient in Cu at 1173°C. The slower the solute diffusion, the higher the maximum temperature for self-organization. For Nb and Mo, macroscopic coarsening was not observed up to the temperatures indicated.[39]

materials. The previously mentioned studies revealed, in particular, the role of solute solubility, solute diffusion, heat of mixing, and mixing and decomposition in displacement cascades on the stabilization of radiation-resistant self-organized nanostructures. There is clearly great interest in extending these studies to the resistance of these nanostructures to swelling and creep.

Nanostructured ferritic alloys

Nanostructured ferritic alloys (NFAs) hold tremendous promise for future fuel cladding and structural materials applications in advanced nuclear fission and fusion reactor concepts. A more comprehensive bibliography on NFAs may be found in the recently published review by Odette et al.[43] NFAs are Fe-Cr–based ferritic, or in some cases ferritic-martensitic[44] alloys with an ultrahigh density of nanometer-sized Y-Ti-O-rich precipitate clusters. NFAs are distinguished from more traditional oxide dispersion steels by a higher number density and smaller size of precipitates, which produce much greater interfacial area available for trapping and recombining point defects.[43,45–48] These alloys have indeed demonstrated outstanding high-temperature properties and remarkable tolerance to irradiation-induced–displacement damage.[43,47–49] Furthermore, NFAs hold tremendous promise for managing high levels of insoluble gases, such as are implanted in fusion energy or spallation neutron irradiation environments.[47]

While NFAs are in the early stages of development, it is increasingly clear that the nanometer Y-Ti-O precipitate clusters are responsible for the outstanding thermal and mechanical properties and good behavior in irradiation environments. As with the earlier examples of planar interfaces and stable, self-organizing nanostructures, the principles of atomic-scale design of interfacial characteristics will be important in optimizing NFAs for nuclear applications. However, detailed understanding of

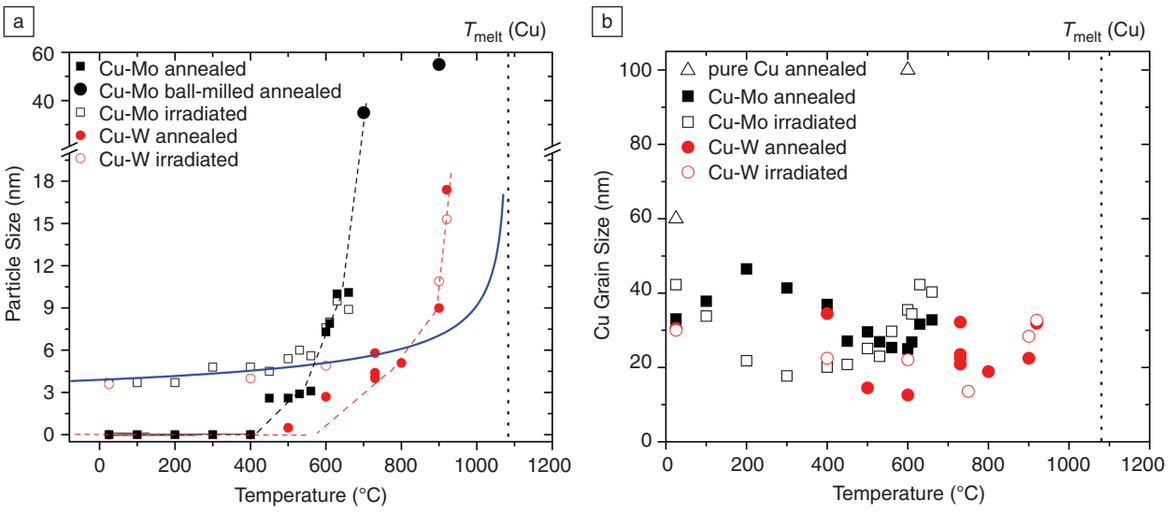

Figure 4. (a) Precipitate size versus temperature during thermal annealing or irradiation at high temperature in Cu-Mo and Cu-W alloys. Blue solid line is a fit to a thermal spike model. (b) Grain size versus temperature during thermal annealing or irradiation at high temperature in Cu-Mo and Cu-W alloys.[40]

the composition and structure of the nanometer-sized Y-Ti-O precipitate clusters, as well as their precipitation and aging (Ostwald ripening) kinetics, is required before atomic-scale design can be fully exploited.

Experimental characterization, predominately by APT, indicate that the Y-Ti-O precipitates have different compositions than stoichiometric oxide phases, which include $Y_2Ti_2O_7$, and orthorhombic Y_2TiO_5, as well as $YTiO_3$ and YTi_2O.[43,50] **Figure 5** shows an example of an enlarged atom image of a nanometer-sized Y-Ti-O precipitate cluster in oxide-dispersion–strengthened steel (Figure 5a), along with the elemental maps for Cr, Y, Ti, and O that show Y and Ti association and the high precipitate number density.[48,51] High-resolution transmission electron microscopy (TEM) studies reveal that larger Y-Ti-O precipitates are semi-coherent, $Y_2Ti_2O_7$ pyrochlore structures,[52,53] consistent with a picture that the Y-Ti-O–rich nanoscale precipitates are coherent, sub-oxide transition phases.

APT also indicates that some Y-Ti-O precipitate clusters have complex core-shell structures[51,54,55] in which the cores contain higher Y concentrations, while the shells are enriched in Ti and O. Yet, as noted by Odette et al.,[43,50] the APT observations are not fully consistent with other characterization techniques, including small-angle neutron scattering, high-resolution TEM, photon spectroscopy, and positron-annihilation spectroscopy.[56] For example, more recent high-resolution TEM studies have indexed both the pyrochlore and orthorhombic phases in extraction replicas, but many of the smaller particles are not easily identified as known oxide phases.[57] Thus, despite a large number of experimental characterization studies, a self-consistent understanding of the character of the nanometer-sized Y-Ti-O precipitate clusters remains lacking, although it is likely that they feature a range of compositions, and perhaps also interfacial structures.

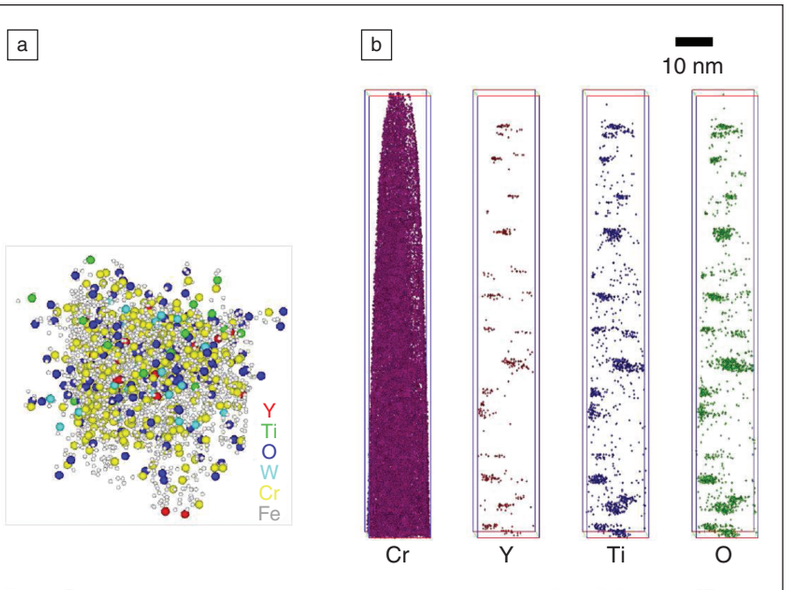

Figure 5. Atom probe tomography reconstructions, as reproduced from References 57 and 61, which show (a) an atom map of a typical Y-Ti-O precipitate; and (b) Cr, Y, Ti, and O elemental maps from nanostructured ferritic alloy 12YWT showing that the elements tend to localize together in clusters. The Cr atoms show the shape of the needle.

Electronic-structure calculations by Jiang and co-workers have focused on investigating the structure and possible precipitation sequence of very small Y-Ti-O clusters in a magnetic bcc Fe matrix.[58] Their results indicate that an energetically favorable clustering sequence exists, beginning with the formation of an O-O pair, which is centered on an Fe lattice site, akin to the structure of a split interstitial dumbbell. The energy of the small cluster is further reduced, indicating an energetically bound configuration, through the addition of nearest neighbor Y atoms, followed by nearest neighbor substitutional O and Ti.[58]

Alinger et al. used lattice Monte Carlo (LMC) simulations to explore the composition of nanometer-sized Y-Ti-O phases.[59] These LMC simulations used a number of simplifying assumptions, including simple pair-bond energies and a simple treatment of lattice strain energy, that remain to be fully assessed. However, the LMC model mapped energetically favorable structures for the Y-Ti-O precipitates, indicative of a strong chemical potential driving force, that are reasonably consistent with the experimental observations. **Figure 6** summarizes the LMC simulation results as a function of effective lattice strain at 0°C (Figure 6a) and as a function of matrix O concentration at 300°C for a fixed lattice strain (Figure 6b).[59] The simulated nanoclusters are roughly spherical (faceted polyhedral), with segregated regions of Y and Ti, a slight enrichment of Ti at the interface, and a Ti to Y ratio of about 2:1, reasonably consistent with the APT characterization. Additional effort is focused on refining the Fe-Y-Ti-O interaction potentials and to evaluate the effect of lattice strain energy directly.

It is tempting to conclude that the segregation of Ti to the Y-O-Fe interface, as well as core-shell structures, may be partially responsible for the good thermal stability and strength of NFAs. Another possibility, raised by Fu et al., is that strong binding between oxygen and vacancies in the Y-Ti-O nanoclusters is critical to providing the structure and thermal stability of the precipitates. They found that oxygen prefers the octahedral interstitial position in the bcc Fe matrix as expected, but that the oxygen strongly binds with neighboring vacancies or Ti atoms.[60] Recent positron-annihilation results, which are very sensitive to vacancies, have reported long-lifetime components in the range of 270–300 ps in NFAs[56,61] but cannot yet be considered conclusive proof of the role of vacancies in the Y-Ti-O precipitates.

In summary, NFAs produced with a high density of the Y-Ti-O nanoscale precipitate clusters have outstanding mechanical properties, remarkable thermal stability, and quite good radiation tolerance. While, the character of the Y-Ti-O nanoscale precipitate clusters remains to be fully resolved, there are indications that the use of atomic-scale design can provide insight into the optimal precipitate characteristics involving the segregation of vacancies, Ti, or other alloying elements to reduce interfacial energies and precipitate coarsening kinetics to optimize the radiation resistance of this emerging class of advanced alloys.

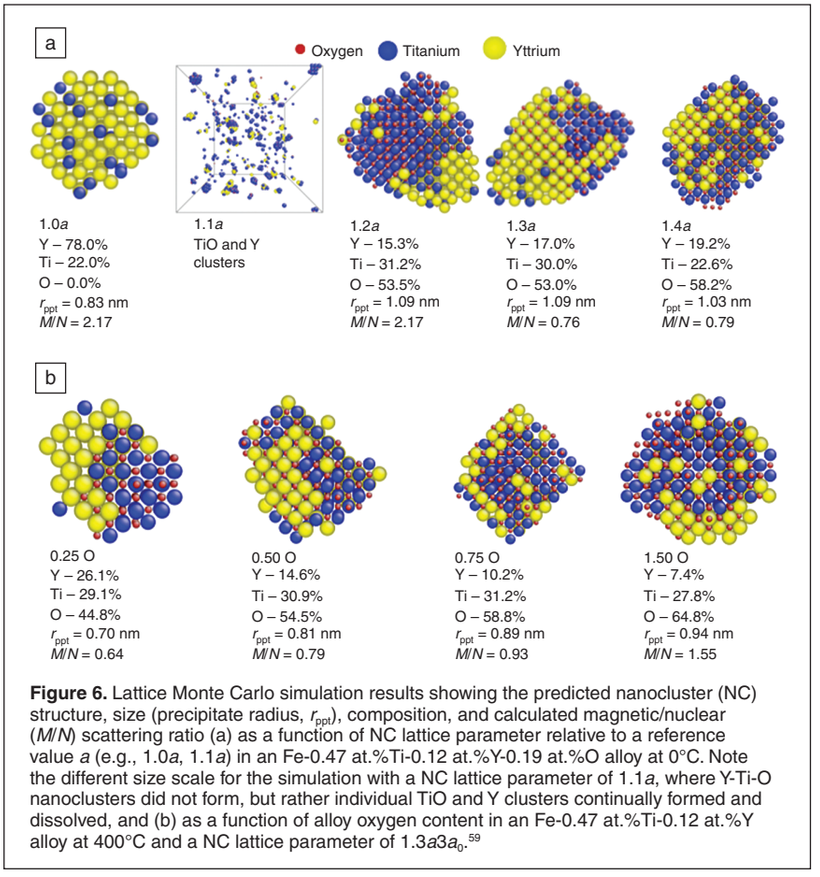

Figure 6. Lattice Monte Carlo simulation results showing the predicted nanocluster (NC) structure, size (precipitate radius, r_{ppt}), composition, and calculated magnetic/nuclear (M/N) scattering ratio (a) as a function of NC lattice parameter relative to a reference value *a* (e.g., 1.0*a*, 1.1*a*) in an Fe-0.47 at.%Ti-0.12 at.%Y-0.19 at.%O alloy at 0°C. Note the different size scale for the simulation with a NC lattice parameter of 1.1*a*, where Y-Ti-O nanoclusters did not form, but rather individual TiO and Y clusters continually formed and dissolved, and (b) as a function of alloy oxygen content in an Fe-0.47 at.%Ti-0.12 at.%Y alloy at 400°C and a NC lattice parameter of $1.3a3a_0$.[59]

Challenges and research directions

The three illustrative examples discussed in this article indicate several challenges to the further development of atomic-scale design of materials for radiation resistance. As was shown in the case of tailoring interface structure, for atomic-scale design to be successful, quantitative structure-property or structure-mechanism relationships for interfaces must be developed and verified. Considerable insight into these relationships has already been gained from previous work, but much of it—being qualitative in nature—is insufficient for atomic-scale design. For example, further work is required to fully understand the structure of interfaces at elevated temperatures or with segregated impurities and how this structure affects interface interactions with extrinsic point and line defects.

Gaining a quantitative understanding of structure-mechanism interactions in interfaces will require modeling methods with improved accuracy able to access large time and length scales. Such a capability will be especially useful in untangling the physics of complex collective

phenomena, such as thermally activated post-cascade demixing at irradiated heterophase interfaces. Correspondingly, verification of insights gained from modeling requires experimental techniques with greater spatial and temporal resolution.

Finally, applying atomic-scale design to create real, physical materials calls for improvements in the control of synthesis at all length scales, from the atomic composition of oxide precipitates in oxide dispersion strengthened steels, to the crystallography of individual interfaces, and the microstructure of multiphase composites. One approach to achieving such synthesis is to take advantage of the nanoscale compositional patterning that irradiation may trigger in alloy systems composed of immiscible elements, as discussed in this article. While the control parameters responsible for these self-organization reactions have been identified for simple binary alloys, tailoring the properties of interfaces in these structures is likely to require the use of ternary and other multicomponent alloys. These challenges will make atomic-scale design for radiation resistance a field of intense research in the years to come.

Acknowledgments

M.J.D. acknowledges support from the Los Alamos LDRD program and the U.S. Department of Energy, Office of Science, Office of Basic Energy Sciences under Award No. 2008LANL1026 through the Center for Materials at Irradiation and Mechanical Extremes, an Energy Frontier Research Center. P.B. acknowledges fruitful collaboration with R.S. Averback and support by the U.S. Department of Energy, Office of Basic Energy Sciences under Grant DEFG02-05ER46217 and by the NSF under Grant DMR 08-04615. B.D.W. acknowledges support by the National Science Foundation under contract NSF DMR 0244562 and the U.S. Department of Energy, Office of Fusion Energy Sciences, under grant DE-FG02-04GR54750.

References

1. K. Ehrlich, *J. Nucl. Mater.* **100**, 149 (1981).
2. R.S. Zhou, E.A. West, Z.J. Jiao, G.S. Was, *J. Nucl. Mater.* **395**, 11 (2009).
3. L.K. Mansur, *Nucl. Technol.* **40**, 5 (1978).
4. V. Fidleris, *At. Energ. Rev.* **13**, 51 (1975).
5. T. Allen, H. Burlet, R.K. Nanstad, M. Samaras, S. Ukai, *MRS Bull.* **34**, 20 (2009).
6. Y. Guerin, G.S. Was, S.J. Zinkle, *MRS Bull.* **34**, 10 (2009).
7. S.J. Zinkle, *Phys. Plasmas* **12**, 8 (2005).
8. D.R. Olander, "Fundamental Aspects of Nuclear Reactor Fuel Elements," (Technical Information Center, Office of Public Affairs, Oak Ridge, TN, 1976).
9. G.S. Was, *Fundamentals of Radiation Materials Science: Metals and Alloys* (Springer, Berlin, 2007).
10. K.S. Kang, Y.S. Meng, J. Breger, C.P. Grey, G. Ceder, *Science* **311**, 977 (2006).
11. E.P. Wigner, U.S. Atomic Energy Commission, Physics Division (1942).
12. D.J. Bacon, Y.N. Osetsky, *Int. Mater. Rev.* **47**, 233 (2002).
13. K.C. Russell, *Prog. Mater Sci.* **28**, 229 (1984).
14. G.R. Odette, G.E. Lucas, *JOM* **53**, 18 (2001).
15. G. Martin, *Phys. Rev. B: Condens. Matter* **30**, 1424 (1984).
16. B.N. Singh, *Philos. Mag.* **29**, 25 (1974).
17. R.W. Siegel, S.M. Chang, R.W. Balluffi, *Acta Metall.* **28**, 249 (1980).
18. M. Dollar, H. Gleiter, *Scripta Metall.* **19**, 481 (1985).
19. K. Inderjeet, Y. Mishin, W. Gust, *Fundamentals of Grain and Interphase Boundary Diffusion* (Wiley, Chichester, NY, 1995).
20. R.G. Hoagland, R.J. Kurtz, *Philos. Mag. A* **82**, 1073 (2002).
21. Y. Mishin, M. Asta, J. Li, *Acta Mater.* **58**, 1117 (2010).
22. H. Schroeder, W. Kesternich, H. Ullmaier, *Nucl. Eng. Des./Fusion* **2**, 65 (1985).
23. A. Misra, R.G. Hoagland, H. Kung, *Philos. Mag.* **84**, 1021 (2004).
24. A. Misra, M.J. Demkowicz, X. Zhang, R.G. Hoagland, *JOM* **59**, 62 (2007).
25. M.A. Nastasi, J.W. Mayer, J.K. Hirvonen, *Ion-Solid Interactions: Fundamentals and Applications* (Cambridge University Press, Cambridge, NY, 1996).
26. T. Hochbauer, A. Misra, K. Hattar, R.G. Hoagland, *J. Appl. Phys.* **98**, 123516 (2005).
27. X. Zhang, N. Li, O. Anderoglu, H. Wang, J.G. Swadener, T. Hochbauer, A. Misra, R.G. Hoagland, *Nucl. Instrum. Methods Phys. Res., Sect. B* **261**, 1129 (2007).
28. T.E. Mitchell, Y.C. Lu, A.J. Griffin, M. Nastasi, H. Kung, *J. Am. Ceram. Soc.* **80**, 1673 (1997).
29. M.J. Demkowicz, R.G. Hoagland, *Int. J. Appl. Mech.* **1**, 421 (2009).
30. M.J. Demkowicz, R.G. Hoagland, J.P. Hirth, *Phys. Rev. Lett.* **100**, 136102 (2008).
31. M.J. Demkowicz, J. Wang, R.G. Hoagland, in *Dislocations in Solids*, J.P. Hirth, Ed. (Elsevier, Amsterdam, 2008), Vol. 14, pp. 141.
32. K.M. Knowles, *Philos. Mag. A* **46**, 951 (1982).
33. R. Kirchheim, *Acta Mater.* **50**, 413 (2002).
34. A.J. Detor, C.A. Schuh, *Acta Mater.* **55**, 4221 (2007).
35. R.S. Nelson, J.A. Hudson, D.J. Mazey, *J. Nucl. Mater.* **44**, 318 (1972).
36. W. Jaeger, H. Trinkaus, *J. Nucl. Mater.* **205**, 394 (1993).
37. R.A. Enrique, P. Bellon, *Phys. Rev. Lett.* **84** (2000)
38. R.A. Enrique, K. Nordlund, R.S. Averback, P. Bellon, *J. Appl. Phys.* **93**, 2917 (2003).
39. S.W. Chee, B. Stumphy, N.Q. Vo, R.S. Averback, P. Bellon, *Acta Mater.* **58**, 4088 (2010).
40. N.Q. Vo, S.W. Chee, D. Schwen, X. Zhang, P. Bellon, R.S. Averback, *Scripta Mater.* (in press)
41. P. Krasnochtchekov, R.S. Averback, P. Bellon, *Phys. Rev. B: Condens. Matter* **72**, 1 (2005).
42. R.S. Averback, T. Diaz de la Rubia, *Solid State Phys.* **51**, 281 (1998).
43. G.R. Odette, M.J. Alinger, B.D. Wirth, *Annu. Rev. Mater. Res.* **38**, 471 (2008).
44. S. Ukai, T. Okuda, M. Fujiwara, T. Kobayashi, S. Mizuta, H. Nakashima, *J. Nucl. Sci. Technol.* **39**, 872 (2002).
45. D.J. Larson, P.J. Maziasz, I.S. Kim, K. Miyahara, *Scripta Mater.* **44**, 359 (2001).
46. M.J. Alinger, G.R. Odette, D.T. Hoelzer, *J. Nucl. Mater.* **329/333**, 382 (2004).
47. T. Yamamoto, G.R. Odette, P. Miao, D.T. Hoelzer, J. Bentley, N. Hashimoto, H. Tanigawa, R.J. Kurtz, *J. Nucl. Mater.* **367–370**, 399 (2007).
48. D.T. Hoelzer, J. Bentley, M.A. Sokolov, M.K. Miller, G.R. Odette, M.J. Alinger, *J. Nucl. Mater.* **367**, 166 (2007).
49. I.S. Kim, J.D. Hunn, N. Hashimoto, D.L. Larson, P.J. Maziasz, K. Miyahara, E.H. Lee, *J. Nucl. Mater.* **280**, 264 (2000).
50. G.R. Odette, D.T. Hoelzer, *J. Nucl. Mater.* (2010), In press.
51. M.K. Miller, K.F. Russell, D.T. Hoelzer, *J. Nucl. Mater.* **351**, 261 (2006).
52. M. Klimiankou, R. Lindau, A. Moslang, *J. Cryst. Growth* **249**, 381 (2003).
53. M. Klimiankou, R. Lindau, A. Moslang, *Micron* **36**, 1 (2005).
54. E.A. Marquis, *Appl. Phys. Lett.* **93**, 181904 (2008).
55. C.A. Williams, E.A. Marquis, A. Cerezo, G.D.W. Smith, *J. Nucl. Mater.* **400**, 37 (2010).
56. M.J. Alinger, S.C. Glade, B.D. Wirth, G.R. Odette, T. Toyama, Y. Nagai, M. Hasegawa, *Mater. Sci. Eng., A* **518**, 150 (2009).
57. D. Bhattacharyya, P. Dickerson, G.R. Odette (2010), In preparation.
58. Y. Jiang, J.R. Smith, G.R. Odette, *Phys. Rev. B* **79**, 064103 (2009).
59. M.J. Alinger, B.D. Wirth, H.J. Lee, G.R. Odette, *J. Nucl. Mater.* **367**, 153 (2007).
60. C.L. Fu, M. Krcmar, G.S. Painter, X.Q. Chen, *Phys. Rev. Lett.* **99**, 225502 (2007).
61. J. Xu, C.T. Liu, M.K. Miller, H.M. Chen, *Phys. Rev. B* **79**, 020204(R) (2009). □